Combustion and Flue Gas Evolution Characteristics of Rice Husk in Various Mixtures and Layers with Al₂O₃ Particles and Char Prepared with Different Pyrolysis Parameters

Lu Dong,[a,b] Liang Wang,[c] Xuanzhou Huan,[d] Bichen Liu,[e] Baojun Yi,[e] Hongyun Hu,[b] and Fang Huang [a,*]

During pyrolysis and combustion experiments, rice husk and Al₂O₃ were combined in two ways, namely blending (rice husk was blended with Al₂O₃) and covering (rice husk was covered by Al₂O₃) modes, respectively. Rice husk biomass (RHB) char was prepared under different pyrolysis conditions. The resulting combustion characteristics and corresponding gaseous evolution of the biochar were compared. The maximum combustion rate decreased as particles accumulated, causing a shift in the thermo-gravimetric curve to higher temperature ranges. The combustion reaction was hindered in the covering mode. The combustion reactivity of the prepared char decreased as the char preparation time increased. During the char oxidation process, the release amounts of H₂O and CO₂ from char combustion increased first and then decreased, while the release amounts of CO, CH₄, and organic components containing C=O gradually decreased with increasing char preparation time. Char prepared with the covering mode exhibited higher burn-out rates and combustion indices but lower activation energies required for combustion reaction. Additionally, the covering mode delayed the timely release of gases from the biomass heating in air, and the quantity of combustion gas released from the char produced at covering mode was greater than that released from the char produced at blending mode. The results obtained can improve the understanding of stacked biomass particles combustion process.

*Contact information: a: Hubei Key Laboratory of Industrial Fume and Dust Pollution Control, Jianghan University, 8 Sanjiaohu Road, Wuhan 430056, Hubei, China; b: State Key Laboratory of Coal Combustion, School of Energy and Power Engineering, Huazhong University of Science and Technology, Wuhan 430074, China; c: China Power Hua Chuang (Suzhou) Electricity Technology Research Company Ltd., Suzhou 215125, China; d: Xi'an Thermal Power Research Institute Co., Ltd., Xi'an 710032, China; e: College of Engineering, Huazhong Agricultural University, No. 1, Shizishan Street, Hongshan District, Wuhan, 430070, China; *Corresponding author: huangfang5869684@126.com*

INTRODUCTION

Biomass energy possesses abundant reserves, extensive distribution, and the potential for low pollution, making it a renewable and environmentally friendly alternative to fossil resources (Fan *et al*. 2022; Zou *et al*. 2023). However, the various sizes and shapes of biomass may lead to the change of the bulk density of the biomass layer, which may affect the particle heating rate and temperature gradient distribution during pyrolysis,

bioresources.com

prolong the residence time of volatiles on the surface of the particles, and affect the cross-linking reaction between volatiles and coke and the bond breaking mechanism of various functional groups (Soria-Verdugo *et al*. 2023). Onsree *et al*. (2018) studied the effect of size on the pyrolysis of corn residue pellets and eucalyptus wood chips and found that the pyrolysis reaction was significantly delayed during the pyrolysis of specimens having larger particle size. Atreya *et al*. (2017) studied the pyrolysis of wood samples of various sizes (5 to 20 mm) and shapes (spheres, cylinders, cubes, and rectangular blocks) in a vertical tubular furnace. The results showed that the finer particles were pyrolyzed faster, which resulted in less coke and more volatile compounds produced at high temperature. Yu *et al*. (2018) studied the effect of particle size on char yield in a fixed-bed reactor. They found that the effect of particle size was mainly apparent at temperatures below 400 °C. With the particle size increasing, the intra-particle reaction leads to the decrease of tar and gas production and the increase of char production. At higher temperature, the larger surface area provided by the smaller particle size may cause tar cracking and condensation reactions to become dominant, which reduce char and increased gas production.

In engineering applications, biomass pyrolysis involves an oxidation (or partial combustion reaction with limited oxygen), which is facilitated by air in the biomass accumulation gaps. Biomass combustion differs from traditional pulverized coal combustion due to the low bulk density and difficulty of crushing, which requires larger particles to be used for combustion (Farrow *et al*. 2020). Consequently, consideration of the effect of particle bulk density and char pyrolysis conditions on combustion can provide insight into the process of biomass pyrolysis. Some recent experimental investigations have been conducted in this area. Meng *et al*. (2020) investigated the impact of different pine wood and corn straw (50% ratio) sizes ranging from 3 to 8 cm in length on the combustion process in a fixed bed. They found that increasing fuel size to 5 cm enhanced the combustion stability and decreased the emissions of NO. Tanui *et al*. (2020) investigated the influence of particle packing density on wood combustion in a oxy-fuel atmosphere and found that the packing density affected combustion process by changing the combustion conditions and flammability limits; then the burning condition was shifted to fuel-lean side with increasing bed porosity. Zhang *et al*. (2023) found that in the actual combustion, the activation energy in the low-temperature region was lower than that of the theoretical calculation as increasing in the straw-bale fuel density, and the activation energy of wheat-bale fuel in the high-temperature region was lower than that of corn straw-bale fuel. Liang and Singer (2023) used a 3-D, pore-resolving CFD simulation approach to examine the impact of morphology on zone II combustion for biomass char particles (~100 μm). In contrast to larger particles, the sub-millimeter, high aspect ratio biomass char particles exhibited localized reactant penetration into the innermost regions of the particles. Mian *et al.* (2020) investigated the combustion behavior of typical biomass pellets and found that the activation energy of devolatilization stage was enhanced because of the compact physical structure of biomass pellet, and the deoxygention, polymerization, and aromatization reactions were suppressed resulting in higher reactivity of the pellet char than raw biomass char.

In a word, the particle bulk density of biomass may not only affect the biomass pyrolysis but be a critical factor affecting biomass combustion due to the inevitable changes in bed bulk characteristics caused by the different shapes and sizes of biomass particles. In the early stages of biomass combustion, hemicellulose, and cellulose release volatile matter, which ignites after reaching a certain temperature and oxygen level (Marques *et al*. 2019). The heat generated by the combustion of volatile matter provides energy for

bioresources.com

subsequent release and ignition. This process affects the structure of char and its ignition process (Granados *et al*. 2019). The combustion of char is a key aspect of biomass combustion mechanisms. Thermogravimetric and infrared technologies can be combined (TGA-FTIR) to understand the weight loss during biomass (or biochar) combustion and identify volatile gas components online (Varol and Mutlu 2023; Wang *et al*. 2018). Ma *et al*. (2016; 2018) examined the thermal decomposition characteristics of palm waste in the presence of N_2 and N_2/O_2 atmospheres. The results revealed a greater weight loss in air than in N_2, particularly during the combustion stage. CO_2 and H_2O were the primary products in air, with H_2O release concentrated at 200 to 400 °C, although H_2O release was also observed in the high temperature region. CO_2 release were evident during rapid oxidation (139 to 352 °C) and combustion (352 to 780 °C). Volli *et al.* (2021) employed TG-FTIR to examine the pyrolysis of cellulose, lignin, and agricultural residues. Released gases included CO, C=C, CO_2, C=O, C-O, and CH_4 gaseous functional groups with a strong synergistic effect, as shown by the FTIR analysis.

The variety of types, sizes, and shapes of biomass that result in the changes such as bulk density cannot be effectively eliminated, making it necessary to investigate the key issues of biomass combustion under different bulk density conditions. Thus, it is also essential to explore the combustion characteristics of char prepared under various stacked density conditions without changing the number of particles. This study considered the combustion behaviors of biochar prepared by various stacked density conditions and heating times. The weight loss and gas product release characteristics of biochar combustion were studied using TGA-FTIR. Under the same experimental conditions, three stacked density types of samples were created using fine-grained rice husks and Al_2O_3, and the weight loss and gas product release characteristics of rice husks were investigated. The study aimed to refine the nature of the combustion mechanism of biomass in various stacked density.

EXPERIMENTAL

Materials

Rice husk biomass (RHB), which is a conventional agricultural byproduct, was employed as the feedstock in present study. The RHB was crushed to a particle size range of 100 to 200 mesh using a pulverizer, in which a powder particle size between 0.075 and 0.15 mm would be obtained. Al_2O_3 (analytical grade, Sinopharm Chemical Reagent Co., Ltd.) with a particle size range of 1 to 2 mm was selected and heated at 800 °C in a muffle furnace for 3 hours, followed by cooling for later use. The fine particles of Al_2O_3 were obtained in 100 to 200 mesh size range and subsequently subjected to a drying process in a furnace at the temperature of 110 °C for later use. Table 1 presents the proximate analysis, elemental analysis, and the lower heating value (LHV) of RHB.

For the preparation of the biochar samples, a mixture was created by combining about 1 g of RHB and 10 g of Al_2O_3 by thorough two ways of preparation either by thorough mixing (as the blending mode) and in a layered manner (as covering mode), respectively. The blending mode involved adding the Al_2O_3 and RHB into a centrifugal tube in the specified proportions and shaking. After mixing, the mixture sample was added to a ceramic tray and spread. The covering mode involved adding the RHB to a ceramic tray and flattening it; subsequently the Al_2O_3 was evenly deposited onto the surface of RHB at a specific ratio. Upon heating the fixed bed to 600 °C, a continuous stream of high-

purity nitrogen gas was supplied to the system at a flow rate of 1 L/min. The ceramic tray with the mixture sample was expeditiously relocated to the central region of the heating zone, and the timer was initiated to commence the experiment. Following a specified period, the ceramic tray was withdrawn from the heated fixed-bed and subsequently cooled in nitrogen gas. Upon cooling, the ceramic tray was placed in a desiccator, weighed, and recorded. The chars were sieved out of the solid residues and kept in a sample container.

Table 1. Proximate Analysis, Ultimate Analysis, and LHV of the Sample

Sample	Proximate Analysis (wt.% ad)				Ultimate Analysis (wt.% daf)					LHV(MJ/kg)
RHB	M	V	A	FC	C	H	O^a	N	S	17.884
	8.03	67.20	9.66	15.11	55.19	6.93	37.08	0.35	0.46	

Note: M=Moisture, V=Volatile, A=Ash, FC=Fixed carbon, ^{a} Calculated by difference.

Numerous experiments were undertaken to monitor the mass reduction of char during heating and combustion in air, ultimately ascertaining that the duration of the ceramic tray's residence in the furnace was 2 min, 3 min, 4 min, 5 min, and 6 min. The charecterictics of char samples were reported in our previous works (Liu *et al*. 2019, 2023). The blending mode was defined as low stacked density, and the covering mode was defined as high stacked density. The chars prepared at these two stacked densities were labeled RHB-BL-t and RHB-CO-t, where BL stands for low stacked density preparation, CO stands for high stacked density preparation, and t stands for residence time.

TGA-FTIR Experiments

The TGA-FTIR testing apparatus consisted of a thermogravimetric analyzer (TGA, Q600, TA Instruments, USA) and a Fourier transform infrared spectrometer (FTIR, Nicolet iS50, Thermo Fisher Scientific, USA), as reported in our previously study (Liu *et al*. 2023). The samples used were 5 mg of RHB or RHB char, and the temperature for testing was raised from ambient to 900 °C with a heating rate of 20 °C/min using a 100 mL/min flow rate of air, and it was necessary to maintain the temperature of the flue gas connection between TG and FTIR at approximately 220 °C. The combustion analyses were conducted until no further change in mass was detected and the flow rate of air was enough for complete combustion (Rago *et al*. 2022; Mian *et al*. 2020). The air was in excess, and the biomass (or char) was absolutely burned out. The air stream was introduced over the surface of the sample, which was all primary air. The spectrum of the FTIR was recorded within the range 4000 to 400 cm^{-1}, and the scanning time and resolution was set to be 4 s and 4 cm^{-1}, respectively. To investigate the combustion behavior of RHB in different effective bulk density, a blending method and a covering method were used to mix 5 mg RHB and Al$_2$O$_3$ (100-200 mesh) at a mass ratio of 1:5 to create low and high stacked density samples, respectively, defined as RHB-BL and RHB-CO. The TG and DTG characteristics of Al$_2$O$_3$ were also evaluated. The samples weight loss and the gaseous products release characteristics were observed in real-time by TGA-FTIR.

Combustion Characteristic Index

The flammability index (C_r) of biomass was calculated using Eq. 1 (Wang *et al*. 2022),

$$C_r = \frac{(dw/d\tau)_{max}}{T_i^2} \tag{1}$$

where $(dw/d\tau)_{max}$ represents the maximum combustion reaction rate (%/min), and T_i represents ignition temperature (K). The T_i value is often determined by extrapolation of TG-DTG.

The ignition characteristic index (C_i) of biomass was calculated using Eq. 2 (Wang *et al*. 2022),

$$C_i = \frac{(dw/d\tau)_{max} \cdot (dw/d\tau)_{mean}}{T_i} \qquad (2)$$

where $(dw/d\tau)_{mean}$ represents the average burning rate, $mg \cdot min^{-1}$.

The biomass combustion stability discrimination index (R_w) was calculated with Eq. 3 (Xing *et al*. 2019),

$$R_w = 8.5875 \times 10^7 \times \frac{(dw/d\tau)_{max}}{T_i \cdot T_{max}} \qquad (3)$$

where T_{max} is the temperature (°C) at which the maximum burning rate is achieved. A higher combustion stability discriminant index indicates greater combustion stability, which corresponds to better combustion stability of biomass fuel.

The biomass volatilization analysis characteristic index (R_v) was calculated by Eq. 4 (Qian *et al*. 2012),

$$R_v = \frac{(dw/d\tau)_{max}}{T_{max} \cdot \Delta T} \qquad (4)$$

where ΔT is temperature range from the beginning of volatile matter to the maximum rate of volatile matter release, which can be expressed as $\Delta T = T_{max} - T_i$. The larger the volatile property index R_v value, the more easily the volatile matter of the biomass is precipitated, and the better the precipitation performance.

Combustion Kinetics

Equation 5 represents the Coats-Redfern method. This equation is extensively employed for determining kinetic parameters such as activation energy, pre-exponential factor, and reaction order in biomass combustion reaction kinetics with a steady heating rate (Guo *et al*. 2018; Mian *et al*. 2019), as follows,

$$\ln\left(\frac{g(\alpha)}{T^2}\right) = \ln\left[\frac{AR}{\beta E}\left(1 - \frac{2RT}{E}\right)\right] - \frac{E}{RT} \qquad (5)$$

and when

$$n=1,\ g(a) = -\ln(1-a) \qquad (6)$$

$$n \neq 1,\ g(a) = \frac{-\ln(1-a)}{1-n} \qquad (7)$$

where $g(a)$ is a function of conversion rate, α is degree of reaction, T is the thermodynamic temperature (K), A is a frequency factor (s^{-1}), R is the general gas constant (8.314 J $mol^{-1} \cdot K^{-1}$), E is activation energy of reaction ($kJ \cdot mol^{-1}$), and β is a constant heating rate in the combustion process (K/min).

Provided that the heating rate β remains constant, $\ln\left(\frac{g(\alpha)}{T^2}\right)$ and $\frac{1}{T}$ should exhibit a linear relationship upon fitting. During the experiment, it is assumed that multiple reaction stages occur ($n = 0, 0.5, 1, 2,$ and 3), and the optimal reaction stage is determined using the principle of best reaction. The value of E is calculated from the slope of the aforementioned

linear fit, which equals ($-\frac{E}{R}$). The intercept of this linear fit, as the $\frac{2RT}{E}<<1$, and the $\ln\left[\frac{AR}{\beta E}\left(1-\frac{2RT}{E}\right)\right]$ can be regarded as a fixed value. The pre-exponential factor (A) can be determined from the intercept of the linear fit.

RESULTS AND DISCUSSION

TGA-FTIR Evaluation Under Various Stacked Density

　　　　TG/DTG curves were obtained for Al_2O_3, RHB, RHB-BL, and RHB-CO combustion in an air atmosphere, and the results are compared in Fig. 1. A slight weight loss was only observed at temperatures below 200 °C corresponding to a weight loss peak in TG-DTG curves of Al_2O_3 heated in the air atmosphere. This was mainly due to the evaporation of adsorbed water in aluminium oxide particles. For the TG curve of RHB, the weight loss of combustion process contained three stages. The first stage (25 to 218 °C) was attributed to water removal from the sample. The main weight loss of RHB combustion reaction (65.01 wt%, 218 to 390 °C) was mainly attributed to the release and combustion of rice husk volatiles, which accelerated the removal of volatile matter. The weight loss (32.67 wt%, 390 to 520 °C) was mainly due to the residual char oxygen reacting to form gaseous substances (Kopczyński *et al*. 2015; Deng *et al*. 2016). As the temperature further increased, the weight loss was not observed in the TG curve.
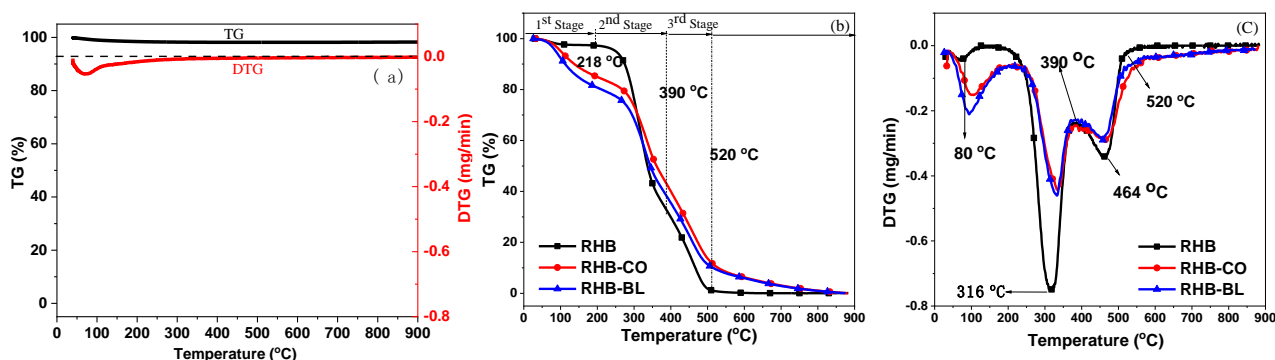
Fig. 1. (a) TG and DTG curves of Al_2O_3, (b) TG and (C) DTG curves of biomass samples prepared under three stacked densities

　　　　Compared with TG/DTG curves of RHB, significant changes in the TG/DTG curves were observed with respect to RHB-BL and RHB-CO. In the first stage, the weight loss of RHB-CO (or RHB-BL) was greater than that of RHB. A small amount of hemicellulose decomposition may occur at the low-temperature region (25 to 218 °C) for RHB-CO and RHB-BL samples due to increased surface temperature of the Al_2O_3 particles added. This may increase heat transfer between particles and promoted the evaporation of water in RHB and Al_2O_3, and decomposition of hemicellulose. The weight loss of RHB-BL was the greatest in the first stage. The peak of the maximum weight loss rate in DTG curves slightly moved to high temperature zone during the first stage. As the temperature continued to increase, the combustion reaction progressed, and during the stage of rapid volatile removal (218 to 390 °C), a shift in the TG curves towards a higher temperature region was observed with respect to RHB-BL and RHB-CO, suggesting that the combustion reaction was delayed, and the weight loss was reduced. The DTG curves

showed that the maximum mass loss rates were decreased in the second stage due to hemicellulose decomposition in the first stage. When the temperature was elevated to 520 °C, the rice husk underwent complete combustion. However, the TG profiles of RHB-BL and RHB-CO exhibited a continual mass loss, albeit at a decreased mass loss rate. This behavior may be attributed to the accumulation of particles, which results in an increase in heat transfer resistance and a consequent sluggish rise in temperature. This, in turn, leads to a more challenging release of volatile matter, which tends to remain on the surface of the particles. Consequently, the combustion reaction of RHB char is impeded and delayed. Compared to the blending mode, the combustion reaction of RHB at the covering mode is characterized by slower heat transfer, less weight loss, and a more pronounced delay in the combustion process.

Gaseous products resulting from RHB, RHB-CO, and RHB-BL displayed similarities. To gain a deeper understanding of the gas composition resulting from the combustion of RHB, along with the origin and distribution of its functional groups, the infrared data depicted in Fig. 2 pertains to the initial combustion peak temperature of RHB in the air atmosphere, which was recorded at 316 °C. On the graph, wave numbers are plotted on the x-axis, while adsorption rate is shown on the y-axis. It is easy to identify several permanent gases, including H_2O, CH_4, CO_2, and CO based on their distinct infrared absorption bands (Fu *et al*. 2010; Ma *et al*. 2018). For instance, the tensile vibration of O-H occurs at 3575 cm^{-1}, which is primarily due to H_2O formed during the oxidation stage through a combustion reaction between the H and O elements (Fu *et al*. 2010). The stretching vibration of CH_4 associated with C-H bond is observed at 2823 cm^{-1} and is primarily due to the decomposition of methoxy, methyl, and methylene (Ma *et al*. 2018). CO_2 is detected at 2308 cm^{-1}, which is primarily the result of the combustion reaction between C and O elements during the oxidation process (Qiao *et al*. 2019). Apart from the permanent gas components, other compounds can be identified in the range of 1800 to 1000 cm^{-1}. The tensile vibration band appeared at 1770 cm^{-1}, which corresponds to the C=O bond. This is often used to identify the presence of carbonyl groups (C=O-) and carboxyl (-COOH) in a variety of aldehydes, ketones, and organic acids (Wang *et al*. 2018). The band at 1178 cm^{-1} indicates the C-O and C-H bonds, as well as the carbon chain skeleton, which includes alkanes, alcohols, ethers, and lipids (Huang *et al*. 2020). Based on the results depicted in Fig. 2, in the air, the main components of RHB combustion are CO_2 at 2308 cm^{-1} and H_2O at 3575 cm^{-1}.
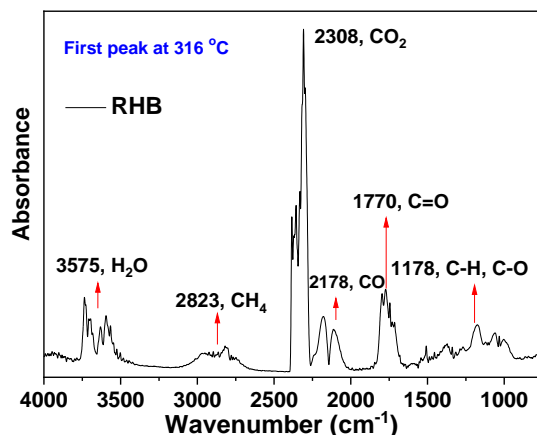
Fig. 2. The FTIR spectra obtained of gaseous products from RHB combustion at the first peak temperature (316 °C)

The Fourier transform infrared (FTIR) spectra of the gaseous products produced by the sample at its characteristic combustion temperature are presented in Fig. 3. When combusted in an air atmosphere, an increase in combustion temperature resulted in the release of a gaseous product peak at 316 °C, corresponding to the maximum weight loss rate $(dw/d\tau)_{max}$ of RHB. The spectrum of RHB at 316 °C shows the presence of CO_2, H_2O, aldehydes, carboxylic acids with C=O chemical group, alkanes, alcohols, ethers, and lipids with C-O or C-H chemical groups, with small amounts of CO and CH_4 also released. The gaseous substances released during the combustion of RHB-BL and RHB-CO at the characteristic temperature are similar to RHB. However, the FTIR spectra of RHB-BL and RHB-CO at the same temperature show reduced release peaks of each gaseous product under particle accumulation, and the absorption peaks of aldehydes, ketones, and organic acids containing C=O functional groups, and alkanes, alcohols, ethers, and lipids containing C-H or C-O functional groups are absent. Comparison of the FTIR spectra of RHB-BL and RHB-CO reveals that the peak corresponding to the release of gaseous products is significantly lower in the spectrum of RHB-CO. This suggests that the accumulated particles (RHB-CO) impede the release rate of gas-phase product and cause some gaseous products to be trapped during RHB combustion.
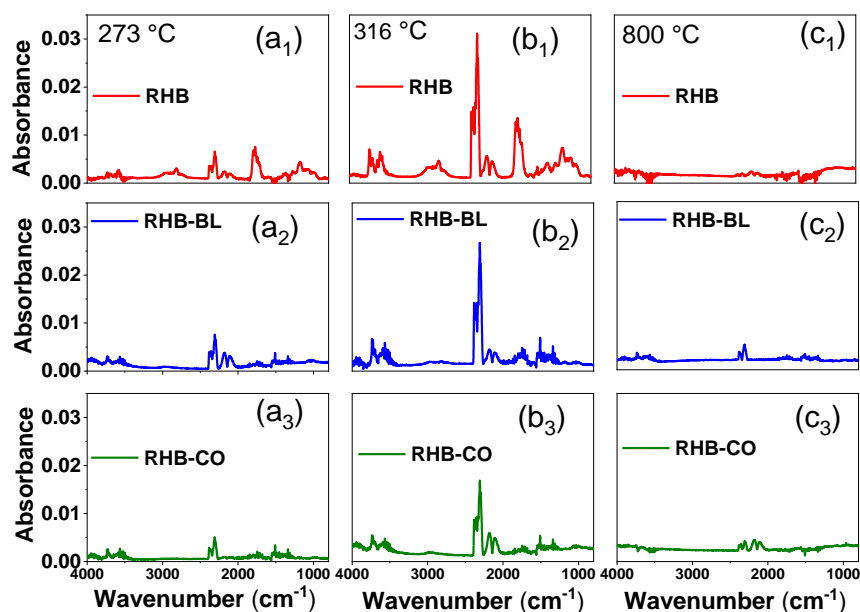
Fig. 3. FTIR spectra of sample combustion gaseous products at different characteristic temperatures. (a_1, a_2, and a_3) ignition stage, (b_1, b_2, and b_3) maximum weight loss rate stage, and (c_1, c_2, and c_3) burnout stage

TGA Analysis of Rice Husk Char Combustion

The reactivity of char during combustion can be significantly influenced by its chemical composition, microcrystalline structure, and porosity (Park and Song 2017; Farrow *et al*. 2020). Nevertheless, the bulk density of particles may alter the accumulation behavior of biomass within the reactor, thereby inevitably impacting the conversion of raw biomass during pyrolysis or combustion, as well as the subsequent oxidation reactions of volatile matter and char. Investigating the combustion characteristics and the evolution of gaseous products of char prepared under different particle stacking conditions can aid in understanding the effects of such accumulation on char structure.

The TG/DTG curves of combustion characteristics of char produced under various accumulation conditions are reflected in Fig. 4. The specific preparation method of the char can be found in a previous study (Liu *et al*. 2019), and the conversion percentages of pyrolytic char for different holding times were obtained and listed, such as 24.0% for RHB-BL-2 char, 17.2% for RHB-CO-2 char, 44.8% for RHB-BL-3 char, 36.2% for RHB-CO-3 char, 53.0% for RHB-BL-4 min char, 49.6% for RHB-CO-4 char, 58.0% for RHB-BL-5 min char, 55.4% for RHB-CO-5 char, 65.2% for RHB-BL-6 char, and 62.0% for RHB-CO-6 char. As the biomass pyrolysis time increased, the char conversion rate increased, and the TG/DTG curve shifted towards a higher temperature region. The char combustion weight loss gradually decreased as the char prepared time increasing, presenting a weight loss step effect. The DTG curves showed the peak of maximum volatile release and combustion decreased and the peak of char (or fixed carbon) combustion increased, which is mainly due to an increase of volatile matter release as char prepared time increased, thus affecting the char oxidation behavior (Farrow *et al*. 2020). The TG/DTG curves of RHB-BL char and RHB-CO char were similar, with the RHB-CO char combustion TG curve on the lower temperature side comparing to the RHB-BL char TG curve. Under the same prepared time, RHB-CO char had a higher value of $(dw/d\tau)_{mean}$ and a higher burnout temperature T_b during combustion in the air atmosphere (as shown in Table 2), indicating an increased char conversion rate at the blending mode. A blending mode resulted in a lower burnout rate for char with low degradable components remaining. The covering mode may hinder heat and mass transfer during pyrolysis, resulting in higher residual organic components in the solid product char. Therefore, the rice husk biomass char produced under the condition of covering mode exhibits a greater $(dw/d\tau)_{mean}$ and a higher T_b.
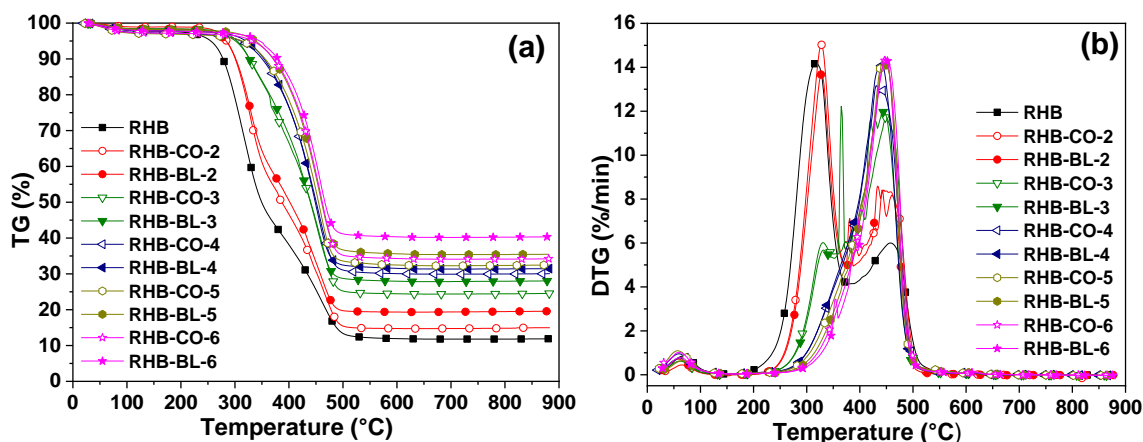
Fig. 4. (a) TG and (b) DTG curves of RHB char oxidation

The combustion characteristics index of RHB, RHB-BL char, and RHB-CO char are shown in Table 2. The T_i range of RHB chars was 293 to 396 °C, while its T_b range was 518 to 595 °C. As the holding time increases, the T_i and T_b of RHB char increase, which may be due to the decreasing of volatile matter in biomass char (Liu *et al*. 2019, 2023). It was observed that the char combustion characteristic index including C_i, C_b, R_w, and R_v decreased gradually with increased biomass pyrolysis holding time. Compared with the combustion characteristics of RHB-BL char at the same holding time, RHB-CO char had a lower T_i and a higher T_b. However, RHB-CO char exhibited larger combustion characteristic indices than RHB-BL char under the same holding time. The slow heat

transfer and volatile matter release during the pyrolysis of RHB-CO may lead to an easy cross-linking reaction, which enhances its char activity and improves the RHB-CO char combustion characteristics.

Table 2. Combustion Characteristics of RHB Char

Sample	T_i (°C)	T_{max} (°C)	T_b (°C)	C_i	C_b	R_v/×10^{-4}	R_w/×10^3
RHB	274.1	315.7	567	3.93	1.88	10.7	14.0
RHB-CO-2	293.6	326.9	521	3.53	1.74	13.8	13.4
RHB-BL-2	294.7	326.9	502	2.99	1.58	12.1	12.1
RHB-CO-3	298.5	331.7	554	2.45	1.38	11.2	10.7
RHB-BL-3	299.1	329.9	540	2.28	1.35	11.0	10.4
RHB-CO-4	372.2	430.9	562	1.62	1.00	5.46	7.39
RHB-BL-4	378.4	440.1	551	1.59	0.98	5.19	7.27
RHB-CO-5	385.5	447.6	594	1.54	0.98	5.22	7.22
RHB-BL-5	386.2	446.9	588	1.45	0.95	5.20	7.02
RHB-CO-6	394.7	448.6	567	1.43	0.92	5.96	6.98
RHB-BL-6	395.4	448.6	565	1.28	0.91	5.95	6.87
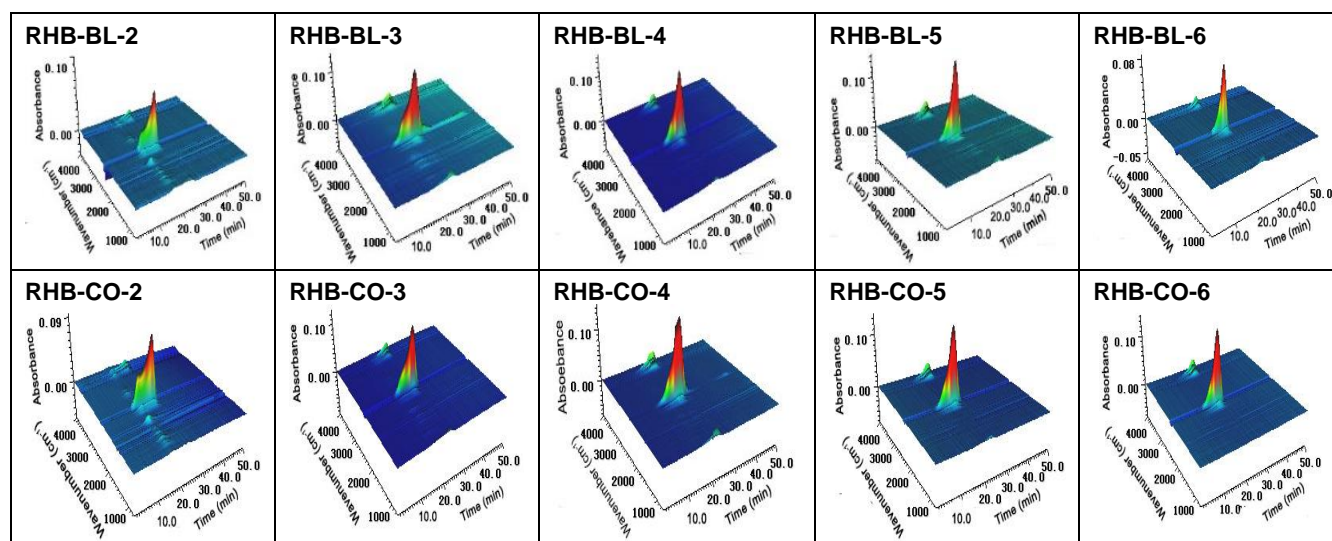
Fig. 5. 3D FTIR evaluation of RHB char combustion gas products

3D FTIR Evaluation of RHB Char Combustion Gas Products

The three-dimensional Fourier transform infrared (3D FTIR) spectra of rice husk char combustion in an air atmosphere as a function of wavenumber and time are shown in Fig. 5. The gaseous product peaks of RHB-BL char and RHB-CO char at different time points during combustion process exhibited a similar trend. The 3D FTIR spectrum of char combustion gas products revealed two distinct infrared absorption bands at 3400 to 3600 cm^{-1} and 2310 to 2400 cm^{-1}, which can be attributed to H_2O and CO_2, respectively (Kopczyński *et al.* 2015). These findings suggest that H_2O and CO_2 are the primary gaseous products released during char combustion. Moreover, the peak shape gradually transformed from a trapezoidal to a sharp peak, which closely resembles the differential thermogravimetric (DTG) curve as the RHB char prepared time increased.

Evolution of Gas Components Released of RHB Char Combustion

To gain a deeper understanding of the combustion behavior, the evolution of gas components released during the combustion of rice husk char was evaluated as a function of time. The released gas products, namely H_2O, CO_2, CO, CH_4, and C=O contained organic gaseous composition, are displayed in Fig. 6.
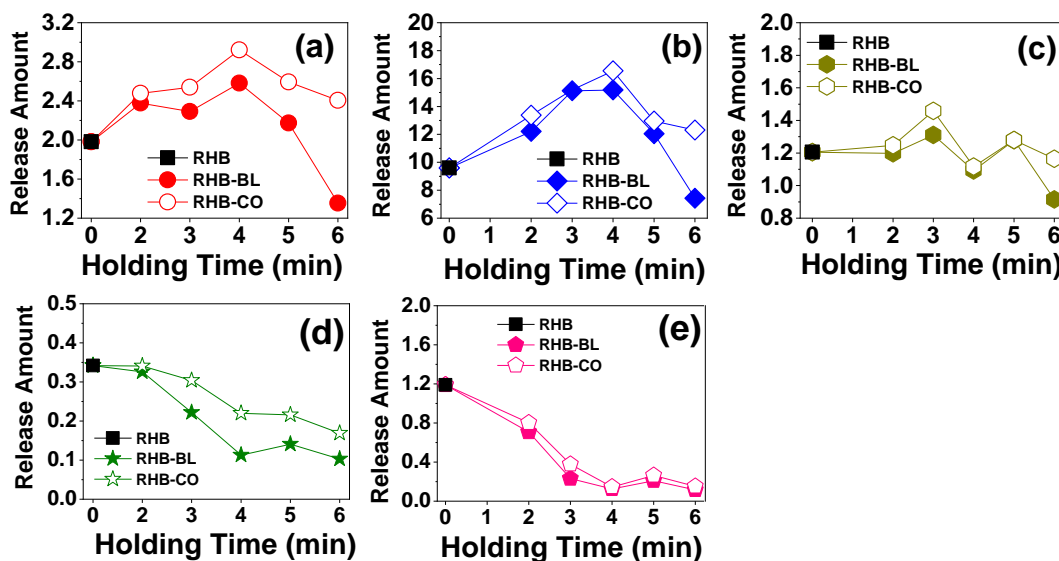
Fig. 6. Evolution of release amount of major gaseous composition of RHB char prepared at various time, (a) H_2O, (b) CO_2, (c) CO, (d) CH_4, and (e) C=O containing organic components

In an air atmosphere, H_2O release is mainly attributed to the oxidation between hydrogen in char and oxygen (Wang *et al*. 2011). With the increase of char prepared time, the amount of H_2O released increased first and then decreased. The release amount of H_2O for char prepared with covering mode is higher, which is mainly caused by the higher content of organic components containing hydrogen and oxygen functional groups in the char prepared with covering mode. This may be attributed to the blocking of pyrolysis heat transfer of rice husk particles, thus resulting in more hydrogen and oxygen functional groups retained on RHB-CO char.

The release of CO_2 is primarily attributed to the decarboxylation and decarbonylation reactions. The temperature range of CO_2 liberation corresponds to the rapid devolatilization (250 to 370 °C) and fixed carbon combustion stage (370 to 500 °C). The amount of CO_2 release exhibited an initial increase, followed by a decrease as the RHB char prepared time increased. A maximum CO_2 release is observed during the combustion of the char produced at the initial stage of carbonization (Liu *et al*. 2019, 2023). Elemental analysis has shown that RHB has a high carbon content of 55.2% (Liu *et al*. 2019). Whether carbon originates from volatile matter or char, it undergoes oxidation with oxygen in the air transformed into gaseous CO_2. Notably, the CO_2 release amount during the combustion of RHB-CO char was greater compared to that of RHB-BL char. This finding suggests that covering mode delays the formation of char and impedes the thermal decomposition of carbonyl/carboxyl release.

The CO formation pathway can originate from the secondary cracking of intermediate products containing aldehydes, such as furfural, furan, and aldehydes, or from incomplete combustion reactions involving decarbonylation (Gao *et al*. 2013; Meng *et al*.

2013). As the RHB char prepared time increased, the quantity of released CO slightly decreased. In comparison to the amount of CO released during the combustion of RHB-BL char, the quantity of CO released from RHB-CO char was higher, consistent with the findings regarding CO_2 evolution.

CH_4 was predominantly produced through the decomposition of three functional groups, such as methoxy (-OCH$_3$), methyl (-CH$_3$), and methylene (-CH$_2$-). The cleavage of -CH$_3$ and -CH$_2$- linked to the side chains of lignin, cellulose, and hemicellulose results in the greater production of CH_4 (Yang *et al*. 2007; Wang *et al*. 2014; Ma *et al*. 2018). The main peak of CH_4 release occurred at a temperature range of 200 to 400 °C. However, the amount of CH_4 released was significantly lower than that of H_2O and CO_2, as the char combustion reaction was more conducive to the formation of H_2O and CO_2. The concentration of H_2O and CO_2 increased, which decreased the concentration of CH_4. With the increase of the RHB char prepared time, the -OCH$_3$, -CH$_3$, and -CH$_2$- components were gradually volatilized and released during the char prepared process. Therefore, the release amount of CH_4 during the char combustion gradually decreased. The CH_4 release amount of RHB-CO char combustion was higher than that of RHB-BL char combustion, indicating that covering mode severely impeded the thermal decomposition of -OCH$_3$, -CH$_3$, and -CH$_2$- components of RHB.

The organic component that contains C=O is primarily derived from the ring-opening reaction in the dextran unit of cellulose and the sugar unit of hemicellulose. Additionally, a minor fraction of this component arises from the cleavage of aliphatic side chains that are attached to phenylpropane units in lignin (Yang *et al*. 2007). The release of this component occurs predominantly at temperatures ranging from 200 to 400 °C. The evolution of organic components containing C=O is comparable to that of CH_4. As the RHB char prepared time increases, the concentration of organic components containing C=O decreases gradually. The combustion reaction converts more char into H_2O and CO_2, thereby decreasing the concentration of organic components containing C=O. Furthermore, compared to RHB-BL char, RHB-CO char releases a greater amount of the C=O organic component, suggesting that covering mode restricts the heat transfer between particles and the thermal decomposition of organic components containing C=O.

The combustion mechanism diagram for char samples prepared at different time and bulk density is depicted in Fig. 7. The arrows in the figure correspond to variations in gas composition, with the color indicating the extent of change. Additionally, the thickness of the arrows represents difference in the quantity of gas released. Gas release during pyrolysis was more facile under blending mode conditions. Conversely, particle in covering mode may impede the volatilization of gases during pyrolysis of rice husks (RHB). Thus, higher bulk densities increase the likelihood of secondary reactions in char. A comparison of char samples prepared at blending versus covering mode reveals that the char prepared at covering mode exhibits higher burn-out rates and yield larger quantities of gas products.
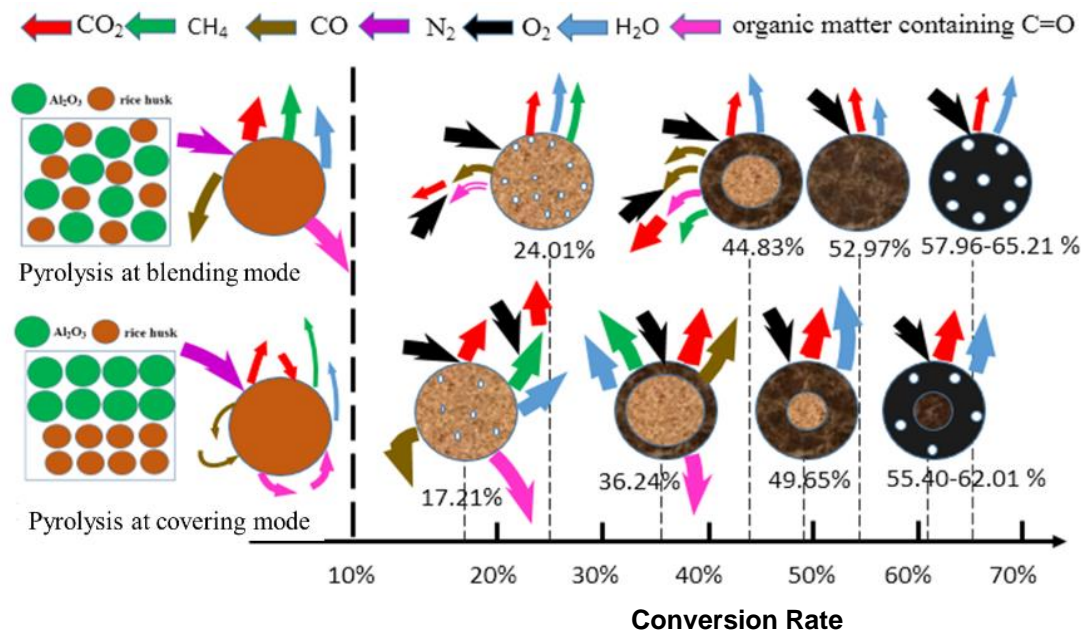
Fig. 7. RHB char combustion mechanism. The thickness of arrow represents difference in the release amount of gas

Distribution of Apparent Activation Energy of RHB and RHB Char Combustion

The variation of E during the combustion of RHB-BL and RHB-CO chars with respect to the conversion rate is depicted in Fig. 8. The distribution of E indicates that three distinct stages of the RHB combustion process can be classified as follows: (1) $0.05 < \alpha < 0.3$; (2) $0.3 < \alpha < 0.7$; and (3) $0.7 < \alpha < 0.9$. In the range of $0.05 < \alpha < 0.3$, E increased from 69.9 to 85.6 kJ·mol^{-1}. This stage is primarily associated with the decomposition of hemicellulose and weakly bonded functional groups (such as hydroxyl, carboxy, and methoxy), which undergo cleavage, as reported in the TG analysis of palm shell waste by Ma *et al.* (2018). Within the stage of $0.3 < \alpha < 0.7$, the value of E varied between 30.1 and 72.8 kJ·mol^{-1}. At this stage, weight loss is mainly due to the thermal degradation of cellulose, which is first converted into activated cellulose. During this process, the degree of polymerization and the length of molecular chains in cellulose are significantly reduced, and the ordered crystal structure is also destroyed. Subsequently, the activated cellulose continues to degrade into lower-molecular-weight components, which require lower E, in accordance with the Broido-Shafizadeh kinetic model (Shen and Gu 2009). Within the range of $0.7 < \alpha < 0.9$, there was a significant increase in E. When the conversion extent α was 0.9, the value of E reached 59.5 kJ·mol^{-1}. The weight reduction observed at this stage primarily resulted from the combustion of lignin and char. Lignin possesses a three-dimensional network structure (Munir *et al*. 2009; May *et al*. 2012) and exhibits excellent thermal stability. Moreover, many low-reactive chars are formed at this stage, which increase the value of E.
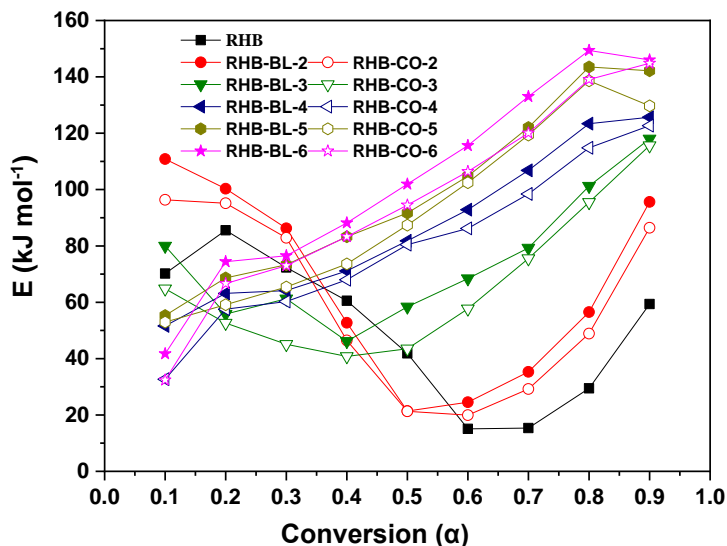
Fig. 8. Analysis of kinetic parameters of RHB and RHB char

Compared to RHB combustion, the activation energy differed significantly for RHB-CO and RHB-BL char combustion at a corresponding conversion extent. As the char prepared time increased, the activation energy required for char combustion increased during the stage of $0.5 < \alpha < 0.9$. The activation energy required for RHB-CO char combustion was lower than that of RHB-BL char combustion at the same prepared time, suggesting that the residual organic components in char prepared at covering mode were relatively high. As a result, RHB-CO char was more easily thermally degraded and ignited compared to RHB-BL char combustion. The combustion index was also larger, which implies that char reaction required lower activation energy in the covering mode. Additionally, the covering mode impedes the heat transfer of particles and increases the possibility of secondary reactions of char. This, in turn, reduces the activation energy required for char combustion reactions.

CONCLUSIONS

1. The ignition and burnout ranges of rice husk biomass (RHB) chars were 293 to 396 °C and 518 to 595 °C, respectively. As the holding time increased, the ignition and burnout temperature of RHB char increased, which may be due to the decreasing of volatile matter in biomass char. The char combustion characteristic index values (for example, the flammability index, ignition characteristic index, combustion stability discrimination index, and volatilization analysis characteristic index) decreased gradually with the biomass pyrolysis holding time increasing.

2. In comparison to char produced at the condition of blending mode, char produced at a covering mode exhibited a greater susceptibility to ignition, higher burn-out rates, and larger combustion indices. The covering mode of biomass particles may result in a lower diffusion rate of gaseous products.

3. Combustion of RHB char did not exhibit significant absorption peaks of products containing organic matter. The evolution pattern of gaseous products with various RHB char was highly similar to the DTG curve. Furthermore, the gaseous products released

from char produced at the condition of covering mode exhibited a greater release amount compared to those from a blending mode char.

4. The activation energy required for the combustion of char prepared in covering mode was lower in comparison to that of char prepared in blending mode.

ACKNOWLEDGMENTS

REFERENCES CITED

Atreya, A., Olszewski, P., Chen, Y., and Baum, H. R. (2017). "The effect of size, shape and pyrolysis conditions on the thermal decomposition of wood particles and firebrands," *International Journal of Heat and Mass Transfer* 107, 319-328. DOI: 10.1016/j.ijheatmasstransfer.2016.11.051

Deng, S., Wang, X., Tan, H., Mikuli, H., Yang, F., Li, Z., and Duic, N. (2016). "Thermogravimetric study on the co-combustion characteristics of oily sludge with plant biomass," *Thermochimica Acta* 633, 69-76. DOI: 10.1016/j.tca.2016.03.006

Farrow, S. T., Sun, C., Liu, H., Manquais, K. L., and Snape, C. E. (2020). "Comparative study of the inherent combustion reactivity of sawdust chars produced by TGA and in the drop tube furnace," *Fuel Processing Technology* 201, article 106361. DOI: 10.1016/j.fuproc.2020.106361

Fan, Y., Liu, C., Kong, X., Han, Y., Lei, M., and Xiao, R. (2022). "A new perspective on polyethylene-promoted lignin pyrolysis with mass transfer and radical explanation," *Green Energy Environment* 7(6), 1318-1326. DOI: 10.1016/j.gee.2021.02.004

Fu, P., Hu, S., Xiang, J. Li, P., Huang, D., Jiang, L., Zhang, A., and Zhang, J. (2010). "FTIR study of pyrolysis products evolving from typical agricultural residues," *Journal of Analytical & Applied Pyrolysis* 88(2), 117-123. DOI: 10.1016/j.jaap.2010.03.004

Gao, N., Li, A., Quan, C., Du, L., and Duan, Y. (2013). "TG–FTIR and Py–GC/MS analysis on pyrolysis and combustion of pine sawdust," *Journal of Analytical and Applied Pyrolysis* 100, 26-32. DOI: 10.1016/j.jaap.2012.11.009

Guo, L., Zhai, M., Wang, Z., Zhang, Y., and Dong, P. (2018). "Comprehensive coal quality index for evaluation of coal agglomeration characteristics," *Fuel* 231, 379-386. DOI: 10.1016/j.fuel.2018.05.119

Granados, D. A., Basu, P., Nhuchhen, D. R., and Janna, F. C. (2019). "Investigation into torrefaction kinetics of biomass and combustion behaviors of raw, torrefied and char samples, " *Biofuels* 12(6), 633-643. DOI: 10.1080/17597269.2018.1558837

Huang, H., Liu, J., Liu, H., Evrendilek, F., and Buyukada, M. (2020). "Pyrolysis of water hyacinth biomass parts: Bioenergy, gas emissions, and by-products using TG-FTIR and Py-GC/MS analyses," *Energy Conversion and Management* 207, article 112552. DOI: 10.1016/j.enconman.2020.112552

***bioresources*.com**

Kopczyński, M., Plis, A., and Zuwała, J. (2015). "Thermogravimetric and kinetic analysis of raw and torrefied biomass combustion," *Chemical and Process Engineering* 36(2), 209-223. DOI: 10.1515/cpe-2015-0014

Liang, D. and Singer, S. (2023). "Pore-resolving simulations of biomass char particle combustion," *Proceedings of the Combustion Institute* 39, 3293-3302. DOI: 10.1016/j.proci.2022.07.098

Liu, B., Fan, Q., Wu, W., and Hu, Y. (2019). "Structure and reactivity of rice husk chars under different bulk densities," *BioResources* 14(4), 8289-8303. DOI: 10.15376/biores.14.4.8289-8303

Liu, W., Liu, B., Zhang, Y., Yi, B., Hu, H., Fan, Q., Li, C., and Liu, H. (2023). "Evolution of pyrolysis characteristics and gas components of biochar prepared by either mixing or layering rice husk with inert aluminum oxide," *BioResources* 1(18), 1699-1713. DOI: 10.15376/biores.18.1.1699-1713

Ma, Z., Wang, J., Yang, Y., Zhang, Y., Zhao, C., and Yu, Y. (2018). "Comparison of the thermal degradation behaviors and kinetics of palm oil waste under nitrogen and air atmosphere in TGA-FTIR with a complementary use of model-free and model-fitting approaches," *Journal of Analytical and Applied Pyrolysis* 134, 12-24. DOI: 10.1016/j.jaap.2018.04.002

Ma, Z., Sun, Q., Ye, J., Yao, Q., and Zhao, C. (2016). "Study on the thermal degradation behaviors and kinetics of alkali lignin for production of phenolic-rich bio-oil using TGA-FTIR and Py–GC/MS," *Journal of Analytical & Applied Pyrolysis* 117, 116-124. DOI: 10.1016/j.jaap.2015.12.007

Marques, E., Ferreira, T., Pereira, C., Paiva, J. M., and Pinho, C. (2019). "Analysis of kinetic and diffusive data from the combustion of char pellets made with hybrid mixtures," *Energy* 181, 1179-1188. DOI: 10.1016/j.energy.2019.05.188

May, Y. E., Jeguirim, M., Dorge, S., Trouvé, G., and Said, R. (2012). "Study on the thermal behavior of different date palm residues: Characterization and devolatilization kinetics under inert and oxidative atmospheres," *Energy* 44(1), 702-709. DOI: 10.1016/j.energy.2012.05.022

Meng, A X., A, Zhou, W., Yan, A, Y., Ren, B, X., Ismail, T. M., and Sun, R. (2020). "Effects of preheating primary air and fuel size on the combustion characteristics of blended pinewood and corn straw in a fixed bed," *Energy* 210, 118481. DOI: 10.1016/j.energy.2020.118481

Meng, A., Zhou, H., Qin, L., Zhang, Y., and Li, Q. (2013). "Quantitative and kinetic TG-FTIR investigation on three kinds of biomass pyrolysis," *Journal of Analytical & Applied Pyrolysis* 104, 28-37. DOI: 10.1016/j.jaap.2013.09.013

Mian, I., Li, X., D.Dacres, O., Wang, J., Wei, B., Jian, Y., Zhong, M., Liu, J., Ma, F., and Rahman, N. (2020). " Combustion kinetics and mechanism of biomass pellet," *Energy* 205, article 117909. DOI: 10.1016/j.energy.2020.117909

Mian, I., Li, X., Jian, Y., Dacres, O. D., Zhong, M., and Liu, J. (2019). "Kinetic study of biomass pellet pyrolysis by using distributed activation energy model and Coats Redfern methods and their comparison," *Bioresource Technology* 294, article 122099. DOI: 10.1016/j.biortech.2019.122099

Munir, S., Daood, S. S., Nimmo, W., Cunliffe, A. M., and Gibbs, B. M. (2009). "Thermal analysis and devolatilization kinetics of cotton stalk, sugar cane bagasse and shea meal under nitrogen and air atmospheres," *Bioresource Technology* 100(3), 1413-1418. DOI: 10.1016/j.biortech.2008.07.065

Onsree, T., Tippayawong, N., Zheng, A., and Li, H. (2018). "Pyrolysis behavior and kinetics of corn residue pellets and eucalyptus wood chips in a macro thermogravimetric analyzer," *Case Studies in Thermal Engineering* 12, 546-556. DOI: 10.1016/j.csite.2018.07.011

Park, D. K., and Song, E. (2017). "Pyrolysis and char oxidation characteristics of oil shales and coal in a thermogravimetric analyzer," *The Canadian Journal of Chemical Engineering* 95(12), 2367-2373. DOI: 10.1002/cjce.22894

Qiao, Y., Wang, B., Zong, P., Tian, Y., Xu, F., Li, D., Li, F., and Tian, Y. (2019). "Thermal behavior, kinetics and fast pyrolysis characteristics of palm oil: Analytical TG-FTIR and Py-GC/MS study," *Energy Conversion and Management* 199, article 111964. DOI: 10.1016/j.enconman.2019.111964

Qian, W., Xie, Q., Huang, Y., Dang, J., Sun, K., Yang, Q., and Wang, J. (2012). "Combustion characteristics of semicokes derived from pyrolysis of low rank bituminous coal," *International Journal of Mining Science and Technology* 22(5), 645-650. DOI: 10.1016/j.ijmst.2012.08.009

Rago, Y. P., Collard, F. X., Gorgens, J. F., Surroop, D., and Mohee, R. (2022). "Co-combustion of torrefied biomass-plastic waste blends with coal through TGA: Influence of synergistic behaviour," *Energy* 239, article 121859. DOI: 10.1016/j.energy.2021.121859

Shen, D. K., and Gu, S. (2009). "The mechanism for thermal deomposition of cellulose and its main products," *Bioresource Technology* 100, 6496-504. DOI: 10.1016/j.biortech.2009.06.095

Soria-Verdugo, A., Cano-Pleite, E., Passalacqua, A., and Fox, R. O. (2023). "Effect of particle shape on biomass pyrolysis in a bubbling fluidized bed, " *Fuel* 339, article 127365. DOI: 10.1016/j.fuel.2022.127365

Tanui, J. K., Kioni, P. N., Mirre, T., Nowitzki, M., and Karuri, N. W. (2020). "The influence of particle packing density on wood combustion in a fixed bed under oxy-fuel conditions," *Energy* 194, article 116863. DOI:10.1016/j.energy.2019.116863

Varol, E. A., and Mutlu, Ü. (2023). "TGA-FTIR analysis of biomass samples based on the thermal decomposition behavior of hemicellulose, cellulose, and lignin," *Energies* 16(9), article 3674. DOI: 10.3390/en16093674

Volli, V., Gollakota, A. R. K., and Shu, C. M. (2021). "Comparative studies on thermochemical behavior and kinetics of lignocellulosic biomass residues using TG-FTIR and Py-GC/MS," *Science of The Total Environment* 792, article 148392. DOI: 10.1016/j.scitotenv.2021.148392

Wang, S., Guo, X., Wang, K., and Luo, Z. (2011). "Influence of the interaction of components on the pyrolysis behavior of biomass," *Journal of Analytical & Applied Pyrolysis* 91(1), 183-189. DOI: 10.1016/j.jaap.2011.02.006

Wang, S., Lin, H., Ru, B., Sun, W., Wang, Y., and Luo, Z. (2014). "Comparison of the pyrolysis behavior of pyrolytic lignin and milled wood lignin by using TG-FTIR analysis," *Journal of Analytical and Applied Pyrolysis* 108, 78-85. DOI: 10.1016/j.jaap.2014.05.014

Wang, T., Zhai, Y., Zhu, Y., Li, C., and Zeng, G. (2018). "A review of the hydrothermal carbonization of biomass waste for hydrochar formation: Process conditions, fundamentals, and physicochemical properties," *Renewable and Sustainable Energy Reviews* 90, 223-247. DOI: 10.1016/j.rser.2018.03.071

Wang, G., Zhang, J., Chang, W., Li, R., and Wang, C. (2018). "Structural features and gasification reactivity of biomass chars pyrolyzed in different atmospheres at high temperature," *Energy* 147, 25-35. DOI: 10.1016/j.energy.2018.01.025

Wang, C., Gao, X., Tang, G., Zhao, L., Mao, Q., Du, Y., and Che, D. (2022). "Thermogravimetric study on oxy-fuel co-combustion characteristics of semi-coke and antibiotic filter residue," *Journal of Thermal Analysis and Calorimetry* 147, 9505-9522. DOI: 10.1007/s10973-022-11220-y

Xing, X., Wang, S., and Zhang, Q. (2019). "Thermogravimetric analysis and kinetics of mixed combustion of waste plastics and semicoke," *Journal of Chemistry* 2019(6), article 8675986. DOI: 10.1155/2019/8675986

Yang, H., Yan, R., Chen, H., Lee, D. H., and Zheng, C. (2007). "Characteristics of hemicellulose, cellulose and lignin pyrolysis," *Fuel* 86(12-13), 1781-1788. DOI: 10.1016/j.fuel.2006.12.013

Yu, J., Sun, L., Berrueco, C., Fidalgo, B., Paterson, N., and Millan, M. (2018). "Influence of temperature and particle size on structural characteristics of chars from beechwood pyrolysis," *Journal of Analytical and Applied Pyrolysis* 130, 127-134. DOI: 10.1016/j.jaap.2018.01.018

Zhang, P., Liu, S., Lu, J., and Wang J. (2023). "Analysis of the combustion process and combustion kinetics of straw-bale fuel," *Biomass Conversion and Biorefinery*. DOI: 10.1007/s13399-023-04101-3

Zou, C., Li, S., Huan, X., Hu H., Dong L., Zhang. H., Dai, Q., and Yao, H. (2023). "The adsorption mechanism of arsenic in flue gas over the P-doped carbonaceous adsorbent: Experimental and theoretical study," *Science of The Total Environment* 895, 165066. DOI: 10.1016/j.scitotenv.2023.165066